Journal of the Meteorological Society of Japan, Vol. 91, No. 4, pp. 539–543, 2013
DOI:10.2151/jmsj.2013-408

NOTES AND CORRESPONDENCE

Reduction of Nonuniform Beam Filling Effects by Vertical Decorrelation: Theory and Simulations

David SHORT, Katsuhiro NAKAGAWA, and Toshio IGUCHI

National Institute of Information and Communications Technology Koganei, Tokyo, Japan

(Manuscript received 13 December 2012, in final form 26 February 2013)

Abstract

Algorithms for estimating precipitation rates from spaceborne radar observations of apparent radar reflectivity depend on attenuation correction procedures. The algorithm suite for the Ku-band precipitation radar aboard the Tropical Rainfall Measuring Mission satellite is one such example. The well-known problem of nonuniform beam filling is a source of error in the estimates, especially in regions where intense deep convection occurs. The error is caused by unresolved horizontal variability in precipitation characteristics such as specific attenuation, rain rate, and effective reflectivity factor.

This paper proposes the use of vertical decorrelation for correcting the nonuniform beam filling error developed under the assumption of a perfect vertical correlation. Empirical tests conducted using ground-based radar observations in the current simulation study show that decorrelation effects are evident in tilted convective cells. However, the problem of obtaining reasonable estimates of a governing parameter from the satellite data remains unresolved.

Keywords radar; attenuation; correction

1. Introduction

The precipitation radar (PR) on the Tropical Rainfall Measuring Mission (TRMM) satellite has been providing unique data on the vertical structure of precipitation systems for the past 15 years. However, the weight and power constraints of this spaceborne radar system require a high-frequency solution (Ku-band) subject to substantial attenuation in heavy precipitation (>10 mm h^{-1}). High-resolution vertical sampling by the PR is used to obtain information on path-integrated attenuation (PIA), a parameter that constrains algorithms designed for attenuation correction, yielding improved accuracy in retrievals of precipitation rate (Iguchi et al. 2009). However, the nonlinear nature of the radar attenuation equation and the power-law relations among specific attenuation (k), radar reflectivity factor (Ze), and precipitation rate (R) are known to induce biases in PIA and the retrieved precipitation rate in the presence of horizontal nonuniformity within the PR field-of-view (FOV), namely the nonuniform beam filling (NUBF) effect (Kozu and Iguchi 1999). High spatial resolution observations from an airborne TRMM PR prototype confirm the presence of the NUBF effect in TRMM PR-scale FOVs and its effects on retrieval algorithms (Durden et al. 1998). In addition, the airborne radar data reveal evidence of vertical decorrelation in the radar reflectivity fields.

A theoretical approach for correcting PIA for the NUBF effect employs an important simplifying assumption: the horizontal structure of precipitation characteristics within the radar FOV is perfectly

Corresponding author and present affiliation: David Short, Science Systems and Application, Inc., 10210 Greenbelt Road, Suite 600, Lanham, Maryland 20706, USA
E-mail: david.a.short@nasa.gov

correlated along the radar-sampled profile (Iguchi et al. 2009), as follows:

$$\rho[k(x, y, n); k(x, y, m)] = 1 \quad (1)$$

where x, y are the horizontal coordinates within the radar FOV, and n, m are any two levels in the radar profile. A height-dependent scaling of the k field is allowed by (1), as explained in the derivation of an associated PIA correction factor, detailed in Iguchi et al. (2009).

This study examines the effects of vertical decorrelation ($0 \leq \rho < 1$) on the PIA correction factor by relaxing the condition expressed by (1).

2. Idealized decorrelation model

Consider an idealized three-dimensional (3D) model of specific attenuation k. At the top level (n = 1), the two-dimensional (2D) domain (x, y, 1) is randomly seeded from $k \sim \Gamma(\theta, \phi)$, where θ and ϕ are the shape and scale parameters of the gamma distribution, respectively. The gamma probability distribution function is as follows:

$$P(k) = \left[\frac{1}{\phi^{\theta} \cdot \Gamma(\theta)}\right] \cdot k^{\theta - 1} \cdot e^{-k/\phi} \quad (2)$$

In addition, subsequent levels are seeded from $k \sim \Gamma(\theta, \phi)$ with a fixed, positive correlation coefficient ρ between adjacent levels.

$$0 \leq \rho[(x, y, n); (x, y, n + 1)] \leq 1 \quad (3)$$

The PIA (x, y, n) for this model is given by the sum of k values at and above the level of interest. The NUBF correction factor for a constrained version of this model, as developed by Iguchi et al. (2009), with $\rho[(x, y, n); (x, y, n + 1)] = 1$ depends on the coefficient of variation (CV) of PIA (x, y, n) over the horizontal domain at the level of interest. The following can be shown by using an expression for the variance of the sum of correlated variables:

$$CV[PIA(n)] = c_1 \cdot \sqrt{[1 + \rho \cdot (n - 1)]/n} \quad (4)$$

where $c_1 = \sqrt{1/\theta}$. The decorrelation effects on the NUBF correction factor are revealed by a decrease in $CV[PIA(n)]$ with increasing n, despite the nonuniformity in k at each level being derived from the same distribution.

3. Simulation of spaceborne radar data using ground-based radar observations

In this study, radar reflectivity factor (Z_e) observations from a C-band radar on Okinawa Island were used. The radar is a component of the comprehensive network of meteorological instrumentation maintained by Japan's National Institute of Information and Communications Technology at its Okinawa Electromagnetic Technology Center. The volume scan data were interpolated onto a 1 km × 1 km Cartesian grid (i, j, l) at three altitudes, l = 3, 2, and 1 km. The observations were performed in June 2004 during a frontal-type rain event with embedded and isolated convection (Shusse et al. 2009).

3.1 Simulation procedure

The gridded radar reflectivity factors $[Z_e(i, j, l)]$ were transformed to Ku-band-specific attenuation $[k(i, j, l)]$, in dB/km, via a power–law relation consistent with the raindrop size distribution in convective rain ($k = 0.000394 Z_e^{\beta}$), with $\beta = 0.7733$ (Short et al. 2012). The attenuation factor (ATF) at l = 1 km includes the sum of k values at and above the lowest level, as follows:

$$\mathrm{ATF}(i, j, 1) = \exp\{-q \times s \times [k(i, j, 3) + k(i, j, 2) + k(i, j, 1)]\} \quad (5)$$

where $q = 0.2 \times \ln(10)$ incorporates a factor of 2 for two-way attenuation, and ln(10)/10 facilitates conversion from Naperian to base 10 logarithms for expressing attenuation in dB. The depth of each attenuating layer is accounted for by s = 1 km. The ATF at l = 2 and 3 km follows a similar pattern by removing the terms below the level of interest.

The measured radar reflectivity factor assumes the ray approximation at each grid cell:

$$Z_m(i, j, l) = Z_e(i, j, l) \times \mathrm{ATF}(i, j, l) \quad (6)$$

The path-integrated attenuation is given by

$$\mathrm{PIA}(i, j, l) = -10 \times \log[\mathrm{ATF}(i, j, l)] \quad (7)$$

A matrix (x, y) of FOV locations at 5-km spacing was centered on the C-band radar location for each volume scan to represent nadir FOV locations for a spaceborne radar with TRMM PR characteristics (Short et al. 2012). The FOV(x, y) locations were restricted to a range of 15–65 km to avoid the ground-based radar cone-of-silence and to minimize the C-band attenuation effects at far ranges.

The quantities averaged over the FOV, denoted by $\langle \cdot \rangle$, were calculated by convolving a two-way illumination function, similar to that of the TRMM PR, with $Z_e(i, j, l)$, $Z_m(i, j, l)$, and $\mathrm{PIA}(i, j, l)$ over each FOV location. The true radar reflectivity factor $\langle Z_e(x, y, l) \rangle$, the measured radar reflectivity factor $\langle Z_m(x, y, l) \rangle$, and $\langle \mathrm{PIA}(x, y, l) \rangle$ at each level were simulated in this

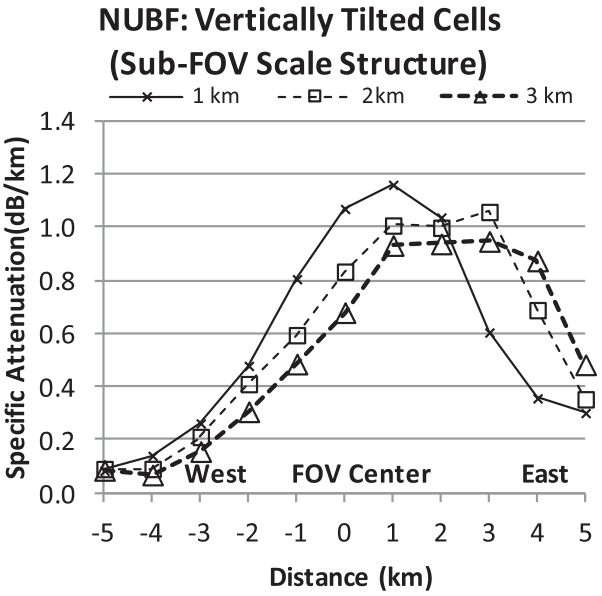

Fig. 1. Composite east–west cross section of specific attenuation of 10 vertically tilted cells.

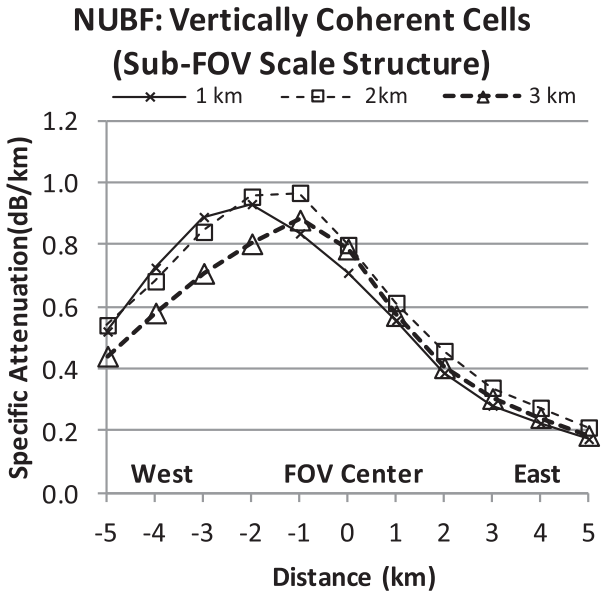

Fig. 2. Composite east–west cross section of specific attenuation of 10 vertically coherent cells.

fashion, as described in Short et al. (2012).

4. Empirical evidence of decorrelation

The gridded radar data provided an approximation of vertical structure in naturally occurring precipitation systems. To distinguish instances of vertical correlation and decorrelation, a special 2D product was created using dBZe(i, j, 1) data from the 1-km level only and by assuming it to be a vertical structure representative over a 3-km-deep layer. The resulting calculations of $\langle Z_e(x, y, l)\rangle_{2D}$, $\langle Z_m(x, y, l)\rangle_{2D}$, and $\langle \mathrm{PIA}(x, y, l)\rangle_{2D}$ were performed for comparison with the 3D results described in Section 3.

A simple algorithm for attenuation correction at the lowest level combines the FOV averages of dBZ_m and PIA to estimate dBZ_e. The presence of NUBF results in an underestimate in this procedure:

$$\mathrm{dB}\langle Z_m(x, y, 1)\rangle + \langle \mathrm{PIA}(x, y, 1)\rangle \le \mathrm{dB}\langle Z_e(x, y, 1)\rangle \quad (8)$$

However, vertical decorrelation mitigates the NUBF effect by reducing the underestimate. On the other hand, vertical coherence leads to similar 2D and 3D underestimates. A comparison of the 2D and 3D simulations revealed 30 FOVs with substantial attenuation (>2 dB/3 km), but varying degrees of decorrelation and sub-FOV structure. An examination of the 2D patterns of dBZ_e over an 11 km × 11 km domain centered on the FOV of interest at the 3-, 2-, and 1-km levels revealed three basic types: tilted rain cells, vertical rain cells, and horizontal gradients. The objective criteria used to distinguish the three types are described in the following sections.

4.1 *Tilted rain cells*

Figure 1 shows the composite east–west cross section of the sub-FOV structure of 10 vertically tilted rain cells where the contrast between the 2D and 3D underestimates was more than 3 dB. At the 1-km level, the maximum specific attenuation was near the FOV center, whereas at the 3-km level, the rain cell was displaced about 2 km eastward, consistent with the vertically tilted cells documented in Shusse at al. (2009).

4.2 *Vertical rain cells*

Figure 2 shows the composite east–west x-section of 10 vertical rain cells where the contrast between the 2D and 3D estimates was less than 0.25 dB in absolute value with $\mathrm{dB}\langle Z_e(x, y, 1)\rangle > 42$. There was some evidence of vertical tilt but not as significant as that shown in Fig. 1.

4.3 *Horizontal gradients*

Figure 3 shows the composite east–west x-section of 10 FOVs where the attenuation exceeded 2 dB/3 km and the contrast between the 2D and 3D underestimates was less than 0.03 dB in absolute value. The

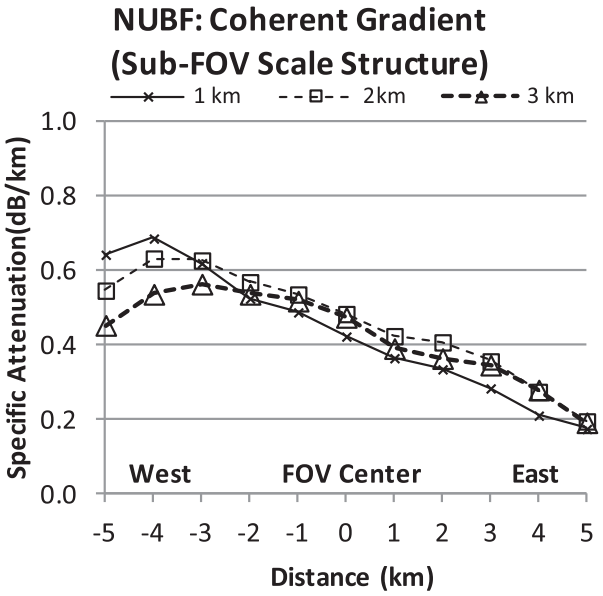

Fig. 3. Composite east–west cross section of specific attenuation of 10 vertically coherent gradients.

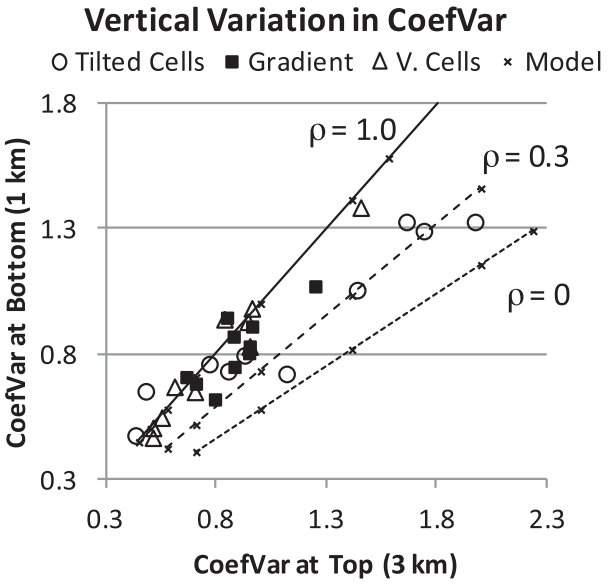

Fig. 4. Sub-FOV coefficient of PIA variation at the top level (3 km) versus bottom level (1 km) for three classes of sub-FOV structure: tilted cells (○), horizontal gradients (■), and vertical cells (△).

sub-FOV gradient and its vertical coherence are reminiscent of the conditions assumed in an early study of the NUBF effect (Nakamura 1991).

4.4 Vertical variation in coefficient of variation

For each of the 30 cases described above (titled cells, vertical cells, and coherent gradients), the coefficient of variation in PIA(x, y, l) was calculated over a 5 km × 5 km domain centered on each FOV location at each of the three data levels. The 5 km × 5 km domain was chosen to match the nominal FOV of the TRMM PR.

Figure 4 shows the comparison of the CV(PIA) values at 1- and 3-km levels for the 30 cases (in three categories) and for the model described in Section 2. The tilted cells (open circles) fall below the 1: 1 line (labeled ρ = 1.0) at an angle closely matched by the model (4) with ρ = 0.3. The coherent vertical cells (open triangles) and coherent gradient cases (solid squares) are clustered just below the 1: 1 line, consistent with a higher correlation between the $k(i, j, l)$ fields at different levels within their respective FOVs.

The NUBF correction factor (CF^*) derived by Iguchi et al. (2009) depends on CV(PIA) and can be expressed as

$$dBZ_e = dBZ_m + PIA \times \{1 + CF^*\} \quad (9)$$

where $CF^* = [CV(PIA)]^2/\beta$.

Under the conditions of sub-FOV uniformity, CV(PIA) and CF^* are zero. The result in these cases indicates that PIA by itself is sufficient to correct Z_m for attenuation. The decorrelation model represented by (4) can be used to illustrate the rate at which CV(PIA) and CF^* approach zero as the number of independent layers, n, increases.

Figure 5 shows the rate at which the normalized CV(PIA) and CF^* factors decrease as the number of independent layers increases. CV(PIA) and CF^* decrease because the PIA values on the x, y grid at any level are due to the sum of k values at and above that level. As more independent layers are added, the spatial variability in the sum (PIA) becomes smoother and CV(PIA) decreases. In the limit $n \rightarrow \infty$, the sum of k values becomes constant over the x, y domain and CV(PIA) becomes zero, as observed in (4) with ρ = 0. The CV(PIA) curve in Fig. 5 can be considered as either a special case with θ = 1 or a general case normalized by $c_1 = \sqrt{1/\theta}$. For n = 3, the normalized CV(PIA) decreases to less than 0.60. This is consistent with the ρ = 0 line in Fig. 4, showing a ratio of 1.3/2.3 = 0.57 for a three-layer model.

5. Discussion and conclusions

The top–down view of a spaceborne radar system provides an opportunity for attenuation correction by cloud and rain hydrometeors, if the radar return from the underlying surface can be measured and its surface

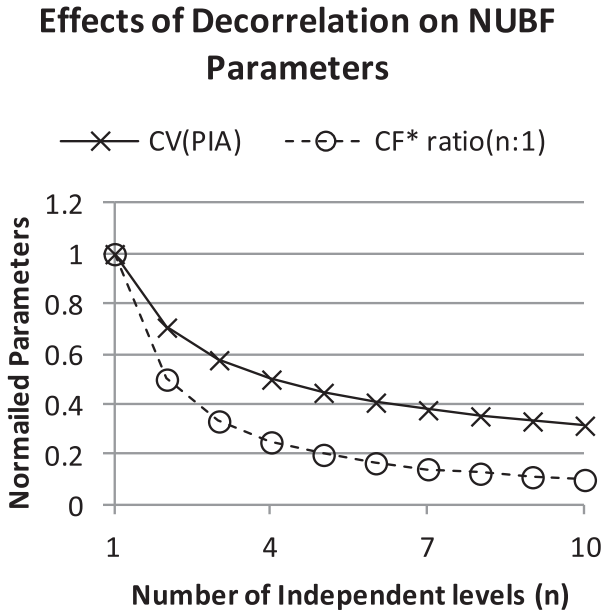

Fig. 5. Number of independent levels versus normalized NUBF parameters CV (PIA) and CF^*, calculated from the idealized model (4) presented in Section 2.

backscattering cross section can be accurately determined. The PIA determined by this surface reference technique is sufficient for attenuation correction when the horizontal sub-FOV structure of hydrometeor characteristics, such as rain rate and specific attenuation, are uniform. The presence of sub-FOV variability, common in convective rain over the 5-km FOV of TRMM PR, introduces the NUBF effect and a bias in the PIA correction procedure.

Iguchi et al. (2009) developed a statistical approach for correcting the NUBF effect under the assumption of a perfect vertical correlation in the sub-FOV horizontal variability along the radar-sampled vertical profile. The theoretical NUBF correction factor, which depends on the sub-FOV coefficient of variation in specific attenuation, has been shown to provide excellent overall results in simulation studies using the ground-based radar observations of naturally occurring precipitation structures (Short et al. 2012).

However, a close examination of vertically tilted rain cells by Short et al. (2012) provided evidence that decorrelation reduces CV(PIA) and the subsequent attenuation correction factor CF^*. The evidence presented in this study is based on simulations of spaceborne radar observations from ground-based radar observations at three levels: 3, 2, and 1 km. The vertical decorrelation effects are evident in these data, and their impacts on NUBF are consistent with a highly idealized statistical CV model. Further simulations with higher-resolution data are required to better quantify the decorrelation effects in various precipitation systems and their mesoscale elements.

However, a greater challenge is to develop procedures for correcting the NUBF effect on attenuation and precipitation-rate retrieval procedures without the direct knowledge of the sub-FOV structure. Simulation studies may provide important clues to help resolve the NUBF issue.

Acknowledgments

The authors thank Professor Toshiaki Kozu of Shimane University for his advice and encouragement.

References

Durden, S. L., Z. S. Haddad, A. Kitiyakara, and F. K. Li, 1998: Effects of nonuniform beam filling on rainfall retrieval for the TRMM precipitation radar. *J. Atmos. Oceanic Technol.*, **15**, 635–646.

Iguchi, T., T. Kozu, J. Kwiatkowski, R. Meneghini, J. Awaka, and K. Okamoto, 2009: Uncertainties in the rain profiling algorithm for the TRMM precipitation radar. *J. Meteor. Soc. Japan*, **87A**, 1–30.

Kozu, T., and T. Iguchi, 1999: Nonuniform beamfilling correction for spaceborne radar rainfall measurement: Implications from TOGA COARE radar data analysis. *J. Atmos. Oceanic Technol.*, **16**, 1722–1735.

Nakamura, K., 1991: Biases of Rain Retrieval Algorithms for Spaceborne Radar Caused by Nonuniformity of Rain. *J. Atmos. Oceanic Technol.*, **8**, 363–373.

Short, D. A., K. Nakagawa, and T. Iguchi, 2012: Empirical test of theoretically based correction for path integrated attenuation in simulated spaceborne precipitation radar observations. *IEEE J. Sel. Topics Appl. Earth Observ.*, **5**, 930–935.

Shusse, Y., K. Nakagawa, N. Takahashi, S. Satoh, and T. Iguchi, 2009: Characteristics of polarimetric radar variables in three types of rainfalls over the East China Sea. *J. Meteor. Soc. Japan*, **87**, 865–875.